Phonon transport in multiphase nanostructured silicon fabricated by high-pressure torsion

Cheng Shao, Kensuke Matsuda, Shenghong Ju, Yoshifumi Ikoma, Masamichi Kohno, and Junichiro Shiomi

View Online   Export Citation   CrossMark

ARTICLES YOU MAY BE INTERESTED IN

Topological effects of phonons in GaN and AlGaN: A potential perspective for tuning phonon transport
Journal of Applied Physics **129**, 085102 (2021); https://doi.org/10.1063/5.0043623

Designing thermal functional materials by coupling thermal transport calculations and machine learning
Journal of Applied Physics **128**, 161102 (2020); https://doi.org/10.1063/5.0017042

Phonon properties and thermal conductivity from first principles, lattice dynamics, and the Boltzmann transport equation
Journal of Applied Physics **125**, 011101 (2019); https://doi.org/10.1063/1.5064602

Phonon transport in multiphase nanostructured silicon fabricated by high-pressure torsion

Cheng Shao,[1] Kensuke Matsuda,[2] Shenghong Ju,[1,3] Yoshifumi Ikoma,[4] Masamichi Kohno,[2,5]
and Junichiro Shiomi[1,a)]

AFFILIATIONS

[1]Department of Mechanical Engineering, The University of Tokyo, 7-3-1 Hongo, Bunkyo, Tokyo 113-8656, Japan
[2]Department of Mechanical Engineering, Kyushu University, 744 Motooka, Nishi-ku, Fukuoka 819-0395, Japan
[3]China-UK Low Carbon College, Shanghai Jiao Tong University, No. 3 Yinlian Road, Lingang, Shanghai 201306, China
[4]Department of Materials Science and Engineering, Kyushu University, 744 Motooka, Nishi-ku, Fukuoka 819-0395, Japan
[5]International Institute for Carbon-Neutral Energy Research (WPI-I2CNER), Kyushu University, 744 Motooka, Nishi-ku,
Fukuoka 819-0395, Japan

[a)]Author to whom correspondence should be addressed: shiomi@photon.t.u-tokyo.ac.jp

ABSTRACT

We present a combined experimental and numerical investigation of phonon transport in multiphase nanostructured silicon. The sample was synthesized by high-pressure torsion with a nominal pressure of 24 GPa. Based on the x-ray diffraction measurement, we have identified the existence of three phases of silicon in the sample: Si-I, Si-III, and Si-XII, with volume fractions of 66%, 25%, and 9% and average grain sizes of 25, 14, and 11 nm, respectively. The measured thermal conductivities of the sample in the temperature range of 150–330 K are on the order of 5 W/(m K) and exhibit weak temperature dependence. A multiscale modeling that incorporates first-principles lattice dynamics, the Monte Carlo ray-tracing method, and effective medium theory was used to understand the mechanism of phonon transport in multiphase nanostructured silicon as well as the weak temperature dependence. We found that the thermal conductivity of single-phase nanostructured silicon decreases with decreasing average grain size and is about an order of magnitude lower than the corresponding bulk counterpart when the average grain size is $\mathcal{O}(10 \text{ nm})$. The weak temperature-dependent thermal conductivity in the nanostructured silicon is attributed to the strong elastic phonon–boundary scattering at the grain boundary. The thermal conductivity predicted from the multiscale modeling matches reasonably well with the measurement. This work provides insights into phonon transport in multiphase nanostructured materials and suggests that the effective thermal conductivity of nanostructured silicon from high-pressure torsion can be further reduced by increasing the volume fractions of the Si-III and Si-XII phases.

I. INTRODUCTION

The ability to effectively reduce a material's thermal conductivity while keeping its electrical properties unchanged is the ultimate goal for thermoelectric materials.[1–3] Due to the relative difference in the mean free paths (MFPs) of electrons and phonons, introducing nanostructures can effectively scatter phonon while affecting less to the electron transport.[4] There are numerous examples that are in line with this idea in recent years, and it has been shown to be an efficient way to reduce the lattice thermal conductivity.[5–8] For example, the thermal conductivities of nanostructured materials like superlattice,[9,10] nanowire,[11] and nano-porous material[12] are about one or two orders of magnitude lower than the bulk counterpart. However, the above-mentioned materials are usually expensive and are difficult to scale up.

On the other hand, materials with intrinsically low thermal conductivities are also important for thermoelectric applications.[13,14] In addition to the conventional materials from the periodic tables, allotropes of the common elements can exhibit low intrinsic thermal conductivity. Those allotropes, which are often found in the group 14 elements, usually have a large unit cell structure and strong anharmonicity.[15] For example, diamond has the largest thermal conductivity in the bulk phase, while its allotrope

amorphous carbon has a thermal conductivity of 0.2–2.2 W/(m K) at room temperature depending on the synthesis method.[16] Silicon (Si) also has many allotropes other than the commonly seen diamond phase (referred to as Si-I phase). Under high pressure, it can also form the body-centered cubic (BC8, referred to as Si-III) phase and rhombohedral (R8, referred to as Si-XII) phase as well as many other intermediate phases.[17] Those allotrope phases can be obtained physically by high pressure compression[18] or chemically by colloidal synthesis.[17] Zhang *et al.* have recently shown that the thermal conductivity of the phase-pure Si-III is 1–2 orders of magnitude lower than the Si-I phase, which is very attractive for applications that require low thermal conductivity like thermoelectrics.[18] Inspired by the low intrinsic thermal conductivity of the allotropes, a nontrivial question is whether we can further reduce its thermal conductivity by introducing nanostructures.

Severe plastic deformation from high-pressure torsion is an ideal way to achieve this goal.[19] During the high-pressure torsion ultra-fine nanograins that are down to the nanometer scale will be formed in the silicon sample.[20] Moreover, multiple metastable phases have been identified during the high-pressure torsion.[21,22] It has been shown that such a nanograined structure has a large impact on the electrical resistance[23] and mechanical strength.[24] However, the thermal properties of such nanostructured materials formed by high-pressure torsion are less explored. The existence of multiple metastable phases also adds complexity to the heat transfer process, and a good model to understand and predict its thermal properties is still missing. Based on the time-domain thermoreflectance measurement, Harish *et al.* have shown that the thermal conductivity of nanostructured silicon by high-pressure torsion is reduced from the 142 W/(m K) in the single crystal to 7.6 W/(m K).[25] However, it is still unclear why the thermal conductivity of the sample that underwent 10 torsion cycles (smaller grain size) is larger than that of 0 torsion cycles (larger grain size).[25] It is also interesting to know how the volume fractions of different phases and temperature affect the thermal transport.

In this study, we systematically explore the thermal transport in nanostructured silicon by combining the experimental measurements and multiscale modeling. The nanostructured multiphase silicon is first synthesized by high-pressure torsion. The phase composition, volume fraction, and the mean grain size distribution are then extracted from the x-ray diffraction (XRD) measurement, while the temperature-dependent thermal conductivities are measured by the laser flash method. First-principles lattice dynamics are carried out to understand thermal transport and the phonon mean free path distributions in the bulk allotropes phase (Si-I, Si-III, and Si-XII), and the effective thermal conductivity of the nanostructured phase with different grain sizes are calculated from the Monte Carlo ray-tracing simulations. We also apply the effective medium theory to predict the thermal conductivities of the multiphase nanostructured materials, and the results agree reasonably well with the measured value in the temperature range of 150–330 K. We reveal that the weak temperature dependence of thermal conductivity of the nanostructured silicon is attributed to the strong phonon scattering at the grain boundary. We also discuss the possibility to further reduce the thermal conductivity of the multiphase nanostructured silicon.

II. METHODOLOGY

A. Sample preparation and thermal conductivity measurement

To prepare nanocrystal silicon, a single crystalline *p*-type Si wafer with a resistivity of >1000 Ω cm was subjected to the high-pressure torsion process. Tungsten carbide anvils with a hole of 0.25 mm in depth and 5 mm in diameter were used for high-pressure torsion processing. The Si wafers were cut into disks with a diameter of 5 mm. The thickness of the sample was measured using an optical microscope. Two disks were then placed into the shallow hole at the center of the anvils and then loaded at 490 kN at room temperature. Under this loading condition, nominal pressure was estimated to be ∼24 GPa. The torsional shear strain was applied by rotating the lower anvil with respect to the upper anvil at a speed of 1 rpm and the sample underwent plastic deformation. After the rotation, the sample was unloaded to ambient pressure and returned to the elastic regime. The loading and unloading times were ∼7 s and ∼2 s, respectively.[21] The sample after the high-pressure torsion process is mechanically stable and can be polished to a mirror-like surface.[21] Details of the sample preparation and the high-pressure torsion facility have been described elsewhere.[21,26] The XRD measurements were performed using RIGAKU SmartLab with Cu K-α radiation. Rietveld analysis using a crushed sample with random textures was carried out in order to estimate the volume fractions of the Si-I and the metastable phases. The thermal conductivity of the sample is calculated by the following formula:

$$k = \alpha c \rho, \tag{1}$$

where α is the thermal diffusivity, c is the heat capacity, and ρ is the density. The thermal diffusivity α was measured using the laser flash method (LFA457, NETZCH) and the heat capacity values are taken from the literature.[27] The density was calculated according to the lattice constant and the volume fractions of each allotropes phase (Si-I, Si-III, and Si-XII). During the laser flash measurement, the top and bottom surfaces of the sample were coated with graphite powder and were irradiated with a pulsed laser. The time-dependent temperature profile of the sample was measured by a refractive index detector and was used to extract the thermal diffusivity. The thermal conductivity was measured in the temperature range of 150–330 K with an increment of 20 K. The temperature was controlled by selectively turning on/off the inflow of liquid nitrogen.

B. Thermal conductivity calculation

The bulk thermal conductivities of three metastable phases of silicon are calculated by anharmonic lattice dynamics with the force constants obtained from first-principles using the Quantum Espresso[28] and ALAMODE packages.[29] The finite-difference supercell method was to obtain the harmonic and cubic force constants. To extract the force constants, a 4 × 4 × 4 supercell was used for Si-I while a 2 × 2 × 2 supercell was used for Si-III and Si-XII due to their larger unit cell structure. The Perdew–Burke–Ernzerhof exchange-correlation function was used for the force constant calculations.

A $2 \times 2 \times 2$ $\boldsymbol{k}$-mesh was used for the first-principles calculations with the kinetic energy cutoff of 60 Ry and charge density cutoff of 400 Ry.

The effective thermal conductivity of nanostructured silicon can be expressed as

$$k_{\text{eff}} = \frac{1}{3} \sum_s \int_\omega C_s(\omega) v_s(\omega) \Lambda_{s,\text{eff}}(\omega) d\omega, \tag{2}$$

where $C_s(\omega)$, $v_s(\omega)$, and $\Lambda_{s,\text{eff}}(\omega)$ are the heat capacity, the group velocity, and the effective mean free path of the phonon mode with frequency ω and branch s, respectively. Assuming that the main scattering processes are the phonon–phonon scattering and phonon–boundary scattering and they are independent events, the effective phonon mean free path in the nanostructures can be obtained from Matthiessen's rule as[30]

$$\Lambda_{s,\text{eff}}(\omega)^{-1} = \Lambda_{s,\text{pp}}(\omega)^{-1} + \Lambda_{s,\text{bdy}}(\omega)^{-1}, \tag{3}$$

where $\Lambda_{s,\text{pp}}(\omega)$ is the bulk phonon mean free path accounting for phonon–phonon scattering obtained from the first-principles calculations. $\Lambda_{s,\text{bdy}}(\omega)$ is the phonon mean free path considering the phonon–boundary scattering process and can be obtained from the Monte Carlo ray-tracing methods as[31]

$$\Lambda_{\omega,\text{bdy}} = \frac{3}{2} L \int_0^{\pi/2} \tau_{12}(\theta) \cos \theta \sin \theta \, d \theta, \tag{4}$$

where $\tau_{12}(\theta)$ is the phonon transmission across the entire nanostructured material with incident angle θ and length L. This transmission is obtained from the Monte Carlo ray-tracing simulations, in which the phonon transmission probability t of a phonon to pass through an internal grain boundary was required as the input. The diffusive mismatch model (DMM) is used to evaluate the phonon transmission probability t of internal boundaries. Since the internal boundaries are formed by materials of the same species, a transmission probability of 0.5 was used for all phonon modes and the direction after scattering is taken to be fully diffuse.[32] In the Results section, we also compared the difference between the DMM (which assumes a constant transmission for all phonon modes) and the frequency-dependent transmission probability model in predicting the effective thermal conductivity of the nanostructured materials.

The average MFP that is weighted by the thermal conductivity of each mode is an important parameter to quantify the length scale of the heat carriers in crystals and can be calculated as

$$\bar{\Lambda} = \frac{\sum_\omega \frac{1}{3} C_\omega v_\omega \Lambda_\omega^2}{\sum_\omega \frac{1}{3} C_\omega v_\omega \Lambda_\omega}. \tag{5}$$

The effective medium theory was used to calculate the thermal conductivity of the nanostructured silicon that was made of Si-I, Si-III, and Si-XII phases. Four different models, parallel model, serial model, Maxwell model, and Bruggeman model were used for comparison.[33] The corresponding formula to calculate the effective

TABLE I. Effective medium models used to predict the effective thermal conductivity of nanostructured silicon.

Model name	Effective thermal conductivity
Parallel model	$\kappa_{\text{eff}} = \sum_i p_i \kappa_i$
Serial model	$k_{\text{eff}} = \left[\sum_i \frac{p_i}{k_i} \right]^{-1}$
Bruggeman model	$\sum_{i=1}^N p_i \left(\frac{\kappa_i - \kappa_{\text{eff}}}{\kappa_i + 2\kappa_{\text{eff}}} \right) = 0$
Maxwell model	$\sum_{i=2}^N p_i \left(\frac{\kappa_i - \kappa_1}{\kappa_i + 2\kappa_1} \right) = \frac{k_{\text{eff}} - k_1}{k_{\text{eff}} + 2k_1}$

thermal conductivity that contains N ingredients are summarized in Table I, in which p_i and κ_i are the volume fraction and the thermal conductivity of species i, respectively, and κ_{eff} is the effective thermal conductivity of the composited material. The parallel model and the serial model are two of the simplest models and are used to estimate the upper and lower bounds of the effective thermal conductivity. The Maxwell model assumes that the inclusions are spatially separated and mutually independent. Therefore, it is typically valid for low volume fraction of the filler (<25%).[34] The Bruggeman model is derived based on a differential approach, and it is in general more suitable for high filler volume fractions.[34] In this work, the volume fractions of the metastable Si-III and Si-XII phases are 25% and 9%, respectively. Therefore, it is reasonable to apply those models to predict the effective thermal conductivity. We note that the thermal resistance at the grain surfaces inside each constituent phase are included in the Monte Carlo ray-tracing simulations, while thermal resistance at the grain surface between different constituent phases are neglected in the effective medium models. There are two reasons for not including the thermal boundaries resistance between different phases in the effective medium models: (1) the domain size of each constituent phase is much larger than the size of the nanograins inside each phase.[35] Thus, the number of grain boundaries between the same phases is much larger than those of boundaries between different phases.[35] (2) The current effective medium models that included the thermal boundary resistance are limited to two-phase composites, and it is nontrivial to extend it into three-phase composites.[36,37]

III. RESULTS AND DISCUSSION

A. Phase composition and grain size distribution

Complex phase transition will occur during severe plastic deformation. In addition to the initial diamond cubic phase (Si-I), the metastable body-centered cubic BC8 (Si-III) and rhombohedral R8 (Si-XII) phases were also formed during severe plastic deformation.[21] The XRD image of the sample is shown in Fig. 1. Other than the conventional peaks of the diamond cubic Si-I, there are additional peaks at angles of 33°, 52°, and 92°, which are attributed to the metastable Si-III and Si-XII phases. Note that the XRD peaks for the Si-III and the Si-XII phases are similar but are still slightly different and thus are able to be separated during post-
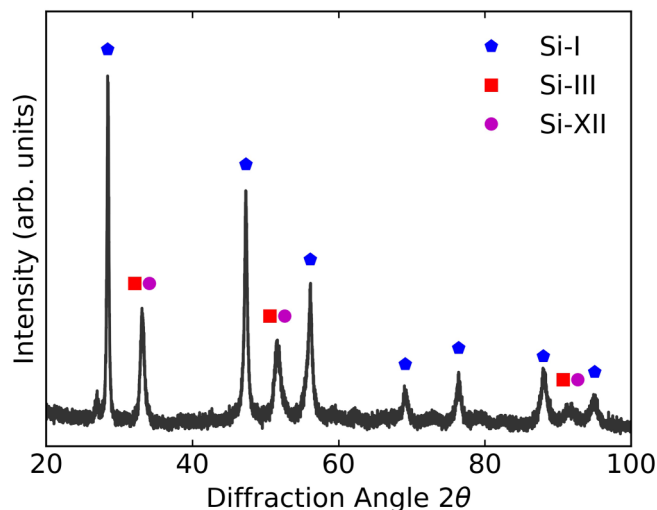
FIG. 1. XRD profile of the samples under ten revolutions of high-pressure torsions. The XRD peaks for the Si-III and the Si-XII phases are similar but are slightly different.

processing. The average grain size of each phase can be determined from the broadening of the XRD peaks as

$$D = \frac{K\lambda}{\beta \cos \theta},$$ (6)

where D is the mean size of each phase, λ is the x-ray wavelength, and β is the full width at half maximum (FWHM) of the peaks. The volume fraction of each phase is determined from relative intensity ratio of those peaks. The compositions and grain sizes obtained by Rietveld analysis are summarized in Table II. The volume fractions for Si-I, Si-III, and Si-XII are 66%, 25%, and 9%, while their average grain sizes are 25, 14, and 11 nm, respectively. For comparison, the average grain size in the as-grown silicon thin film is 9.1 nm,[38] and the grain size is in the range of 5–20 nm in the dc hot press processed sample.[39]

B. Bulk thermal properties

Figure 2(a) shows the bulk phonon properties in three phases of silicon obtained from first-principles calculations. The Si-III phase has the largest thermal conductivity in the temperature range

TABLE II. The volume fractions and the average grain sizes obtained from the XRD profile. The uncertainties in the fitting processes to extract the volume fraction and the grain size are less than 5%.

Phase	Vol. fraction (%)	Grain size (nm)
Si-I	66	25
Si-III	25	14
Si-XII	9	11

of 150–330 K, followed by the Si-XII phase and the Si-III phase. The available thermal conductivities from the experimental measurement are also shown in Fig. 2(a) for comparison.[18,40] The calculated thermal conductivities are slightly lower than the experimentally measured values, which may be due to limitations in the accuracy of the pseudopotential used in this study. For both phases, the thermal conductivity decays monotonically with increasing temperature, which is the typical behavior of crystalline materials. As the temperature increases, more phonons are populated, which leads to stronger phonon–phonon scattering and shorter relaxation time.

We note that the thermal conductivities of Si-III and Si-XII phases are about one order of magnitude smaller than that of the Si-I phase, while the difference in density is less than 10%. The Si-I phase takes a diamond-like crystal structure with two atoms in the primitive unit cell. On the other hand, the Si-III phase takes a body-centered cubic structure with eight atoms in the unit cell, and the Si-XII phase takes a rhombohedral structure with eight atoms in the unit cell. The complex unit cell structures giving rise to larger phase space for phonon scattering as well as the strong anharmonicity are the main reasons for the lower thermal conductivity in the Si-III and Si-XII phases.

Figure 2(b) shows the weighted average MFP $\bar{\Lambda}$ calculated from Eq. (5) in the three different phases of silicon at the temperature range of 150–330 K. The Si-I phase has the largest weighted average MFPs that are in the range of 2000–10 000 nm, followed by the Si-XII phase and the Si-III phase. Similar to the thermal conductivity, the weighted average MFPs in the Si-III and Si-XII phases are also an order of magnitude smaller than that in the Si-I phase. However, even in the Si-III phase, the average MFP is about 200 nm at room temperature, suggesting a large room for reducing the thermal conductivity by introducing phonon–boundary scattering.

Figure 3 shows the normalized cumulative thermal conductivities with respect to phonon MFPs at a temperature of 300 K. In the Si-I phase, phonons with MFPs less than 2130 nm (56.2 nm) contribute to 80% (20%) of the total thermal conductivity, while in Si-III phase, the cutoff MFP for 80% (20%) of the thermal conductivity is 145 nm (9.2 nm), and in the Si-XII phase, it is 594 nm (17.1 nm). In both phases, the MFPs of the dominant heat-carrying phonons span a wide range of spectrum. From the MFP accumulation function, it is expected that a smaller gain size is required for the Si-III phase than the SI-I phase to achieve the same percentage of reduction in the thermal conductivity.

C. Thermal properties in nanostructured silicon

Next, we look at the thermal transport in nanostructured silicon. The temperature-dependent thermal conductivity in nanograin silicon with average grain sizes of 500 nm and 20 nm are shown in Figs. 4(a) and 4(b). The temperature dependence of thermal conductivity is weaker in the nanocrystalline phase, compared with the single-crystal phase as shown in Fig. 2(a), suggesting a non-intrinsic event limiting the phonon relaxation time. As shown in Fig. 2(b), the dominant phonon MFP in the bulk phase is much larger than the average grain size considered here. Therefore, phonon grain boundary scattering is the dominant mechanism to reduce the mean free path. Note that the phonon–boundary
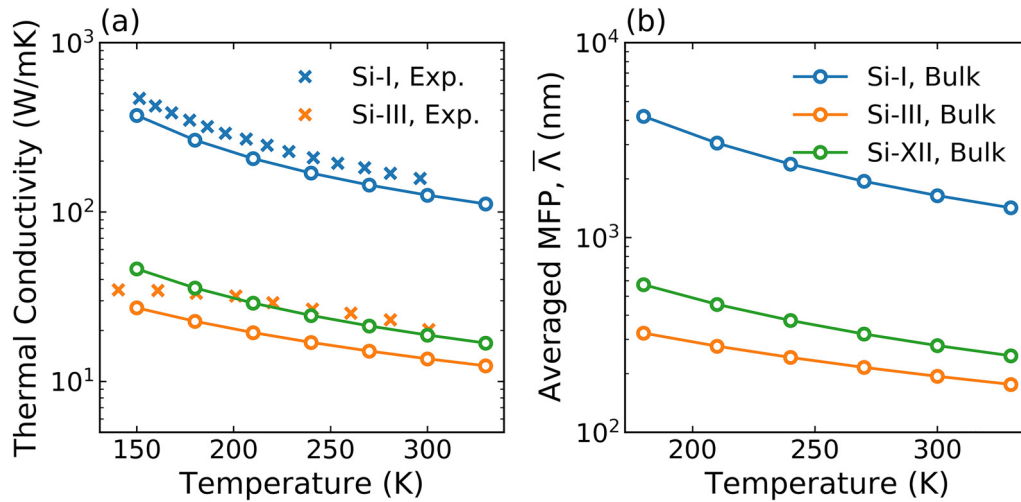
FIG. 2. Temperature-dependent (a) thermal conductivity and (b) weighted average mean free path in different phases of silicon. The experimentally measured thermal conductivities of Si-I[40] and Si-III phases[18] are also shown in (a) for comparison.

scattering is a temperature independent process when assuming elastic scattering, which should be reasonable for silicon at room temperature. Therefore, the overall temperature dependence is weak in the nanostructured silicon compared to the bulk silicon.

The effective thermal conductivities of nanostructured silicon at various grain sizes are shown in Fig. 4(c). The thermal conductivity decreases monotonically with decreasing average grain size. Average grain sizes of 620, 142, and 328 nm are required for the thermal conductivity of the Si-I, Si-III, and Si-XII phases to be

reduced by half. We also calculated the weighted average MFP in nanostructured silicon at different grain sizes and the results are shown in Fig. 4(d). As expected, the weighted average MFP also increases monotonically with the grain size.

The spectral distribution of thermal conductivity as a function of the effective MFP in Si-I silicon at different grain sizes is shown in Fig. 5. In general, reducing the grain size shifts the overall thermal conductivity spectra to the lower mean free path. Taking the 50 nm grain as an example, due to the strong phonon–boundary scattering, the effective MFPs are limited to a narrow range of 5–40 nm, and the major contribution to thermal conductivity comes from phonons with effective MFP of 10–25 nm. The phonon modes with effective MFPs less than 5 nm are mainly optical modes and have negligible contribution to the thermal conductivity even for the smallest grain size of 20 nm considered here

Other than the DMM, recent works also suggest that the phonon transmission at the grain boundary can be frequency dependent, and an empirical frequency-dependent transmission model has been proposed, which takes the form of[41]

$$t(\omega) = \frac{1}{\gamma\omega/\omega_{max} + 1}, \quad (7)$$

where $t(\omega)$ is the transmission of phonon with frequency ω and γ is a parameter that depends on the characteristics of the interface. In this study, we empirically chose the value of γ so that the effective thermal conductivity of the nanostructured silicon agrees with that based on the DMM. We then evaluated how this frequency-dependent transmission model will affect the distribution in the thermal conductivity spectrum in the nanostructured material. The thermal conductivity spectrum with respect to the effective MFP calculated from the DMM and the frequency-dependent transmission model are shown in Fig. 6. For both models, phonons with
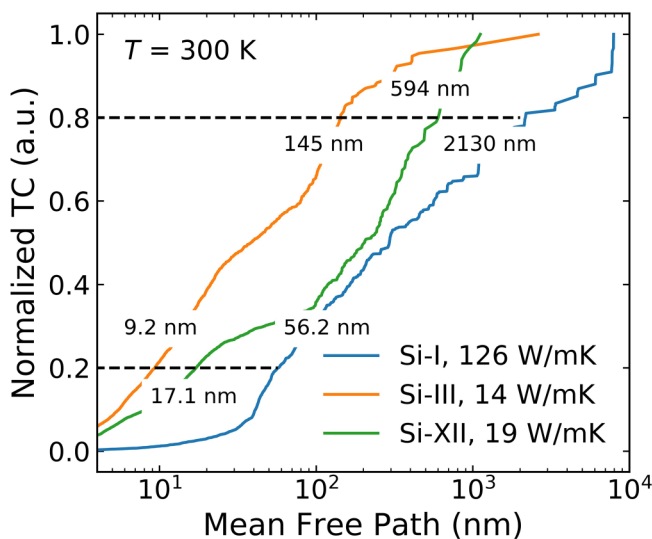

FIG. 3. Phonon mean free path distribution in single-crystal silicon allotropes.
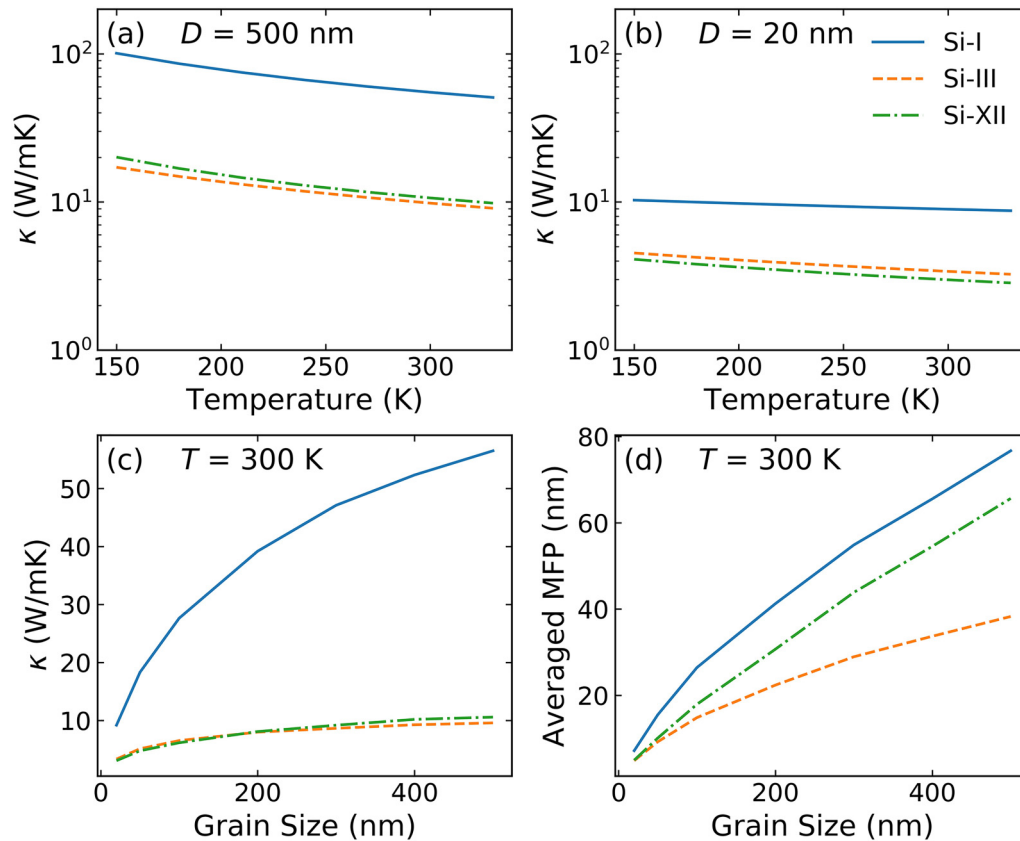
FIG. 4. Temperature-dependent thermal conductivity in nanostructured silicon for average grain sizes of (a) 500 nm and (b) 20 nm. (c) Dependence of the thermal conductivity on the average grain size. (d) The weighted average mean free path (MFP) in nanostructured silicon at different grain sizes.

effective MFP in the range of 10–25 nm have the dominant contribution to thermal conductivity. We note, however, that the largest MFP with a noticeable contribution to thermal conductivity is larger than that with DMM. This is because, in the frequency-dependent transmission model, the low-frequency phonons with large intrinsic MFPs can have a larger transmission and approach to unity in the low-frequency limit.

D. Effective thermal conductivity of nanostructured silicon

We now look at the thermal properties of the multiphase nanostructured silicon. The average grain sizes and their volume fractions are taken from the XRD measurement (as shown in Table II). Note that a more accurate way to study the heat transport in the multiphase nanostructured materials would be applying the direct Monte Carlo simulation to the sample with the exact volume fraction and grain distribution.[42] However, this direct Monte Carlo simulation method is time-consuming and has only been applied to nanostructure material with simple geometry distribution.[43] Recent studies have shown that for single polycrystalline materials, the effective medium theory is sufficient to predict identical results
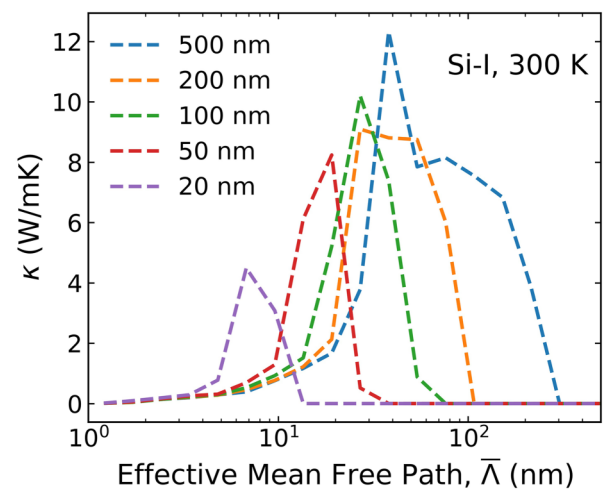

FIG. 5. The spectral distribution of thermal conductivity as a function of the effective mean free path in nanostructure silicon at different grain sizes. The material is Si-I silicon and the temperature is 300 K.
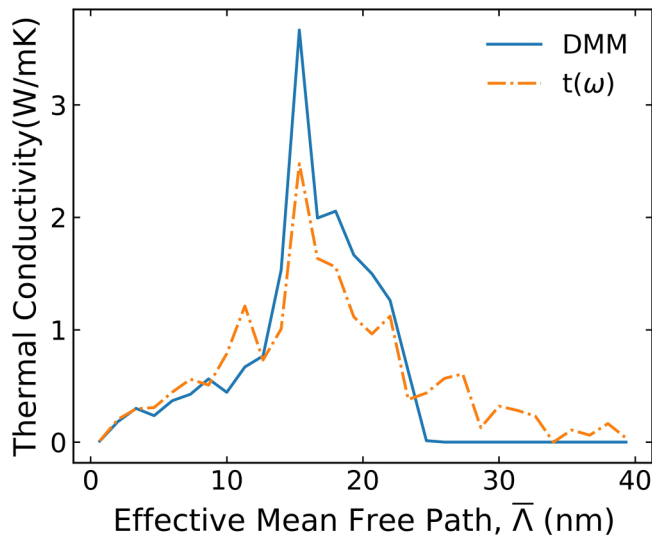
FIG. 6. The thermal conductivity with respect to effective phonon mean free path calculated using the diffusive mismatch model (DMM) and the frequency-dependent transmission model. The material is Si-I silicon and the average grain size is 50 nm.

as the direct Monte Carlo simulations.[44] Here, we combine the Monte Carlo ray-tracing and the effective medium theory to predict the effective thermal conductivity of the multiphase nanostructured silicon. The effective thermal conductivity of each constituent phase is taken from the ray-tracing simulation. The thermal conductivity of each nanostructured silicon as a function of temperature is shown in Fig. 7(a). The thermal conductivities of each constituent phase are 10.5, 2.6, and 1.5 W/(m K) with minor temperature dependence.
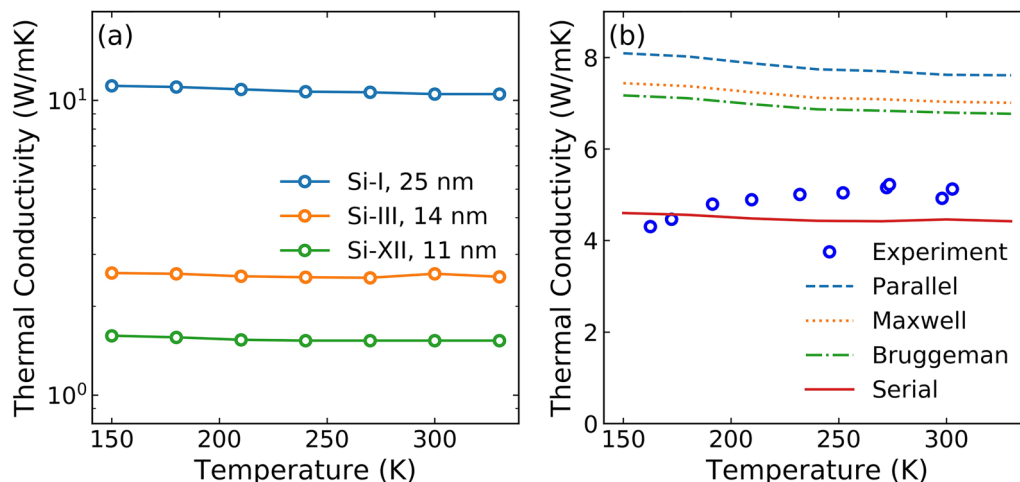
The measured thermal conductivity of multiphase nanostructured silicon as well as the prediction from the different effective medium models at the temperature range of 150–330 K are shown in Fig. 7(b). Note that the average grain size here is in the range of 11–25 nm, which is much smaller than the dominant mean free path in the bulk phase as shown in Fig. 2(b). Therefore, the weak temperature dependence found here again is because the phonon–boundary scattering is the dominant factor that limits the phonon MFP. The slightly positive temperature dependence of the measured thermal conductivity could be caused by the amorphization at the grain boundaries[23] or by the nanostructuring induced modification in the effective Debye temperature.[45]

The measured thermal conductivities fall within the prediction of the serial model and the Bruggeman model but are lower than the parallel model and the Maxwell model. Note that in the real samples, other factors like voids and impurities as well as the electrons can also affect the thermal transport, while those factors are excluded in our model. We first look at the contribution of the free electron to thermal conductivity. The experimentally measured electrical conductivities are in the range of 300–600 S/m. From the Wiedemann–Franz law, $\frac{\kappa}{\sigma} = LT$, where L is the Lorenz number and equals $2.44 \times 10^{-8}\,\mathrm{W\,\Omega\,K^{-2}}$, the contribution of electron to thermal transport should be less than 0.01 W/(m K). Therefore, the thermal transport is dominated by phonons. Based on previous experimental measurements, the porosity ratio in the sample from high-pressure torsion should be less than 10%.[35,46] The reduction of the thermal conductivity for a given porosity depends on the average pore size but considering a range of average pore size from 100 nm to 1 μm, the reduction should not be more than 40%.[47] Therefore, even by taking into consideration the porosity effect in the sample, the measured thermal conductivity would not be larger than that obtained by the parallel model and remains well within the modeled range of thermal conductivities.

Giving the low thermal conductivity of the Si-III and the Si-XII phases, we also expected that one way to further reduce the

FIG. 7. (a) Thermal conductivity of three nanostructured silicon with the average grain size from experimental measurements. (b) The effective thermal conductivity of the multiphase nanostructured silicon at different temperatures.

thermal conductivity is to increase the volume fraction of those two phases. While complete transmission from the Si-I phase to the SI-III requires a pressure as high as 10 GPa,[18] a recent study has shown that it is possible to synthesize the Si-III phase nanoparticle crystal at ambient pressure by the colloidal synthesis routine, which is promising for further reduction of the thermal conductivity of the nanostructure material.[17] In terms of thermoelectric applications, the electrical conductivity and the Seebeck coefficient are other two equally important parameters and thus it is worth to know how they would be affected by the high-pressure torsion. Previous studies have shown that the electrical conductivities of both the normal sample (10 S/m) and the heavily doped sample (10^4 S/m) will be increased by one or two orders of magnitudes after the initial compression process, and both of them return to a value of $\sim 10^3$ S/m after ten revolutions of high-pressure torsion.[23] The impact of the high-pressure torsion on the Seebeck coefficient is left for future investigations.

IV. SUMMARY

In summary, we have combined the experimental and numerical techniques to systematically investigate the thermal transport in multiphase nanostructured silicon in the temperature range of 150–330 K. Based on the XRD measurements, we have identified the phase compositions and volume fractions of the Si-I, Si-III, and Si-XII silicon fabricated from high-pressure torsion. The effective thermal conductivities of each constituent phase as a function of grain size and temperature are calculated from the Monte Carlo ray-tracing method with inputs from first-principles calculations. The thermal conductivity of the multiphase nanostructured silicon from the effective medium models exhibits a weak temperature dependence in the temperature range considered here as a consequence of strong phonon–boundary scattering in the constituent phases. The measured thermal conductivity falls within the values obtained by the effective medium models. Our simulations suggest that the thermal conductivity of the nanostructured silicon can be further reduced by increasing the volume fraction of the Si-III and Si-XII phases.

ACKNOWLEDGMENTS

DATA AVAILABILITY

The data that support the findings of this study are available from the corresponding author upon reasonable request.

REFERENCES

[1]J. Shiomi, APL Mater. **4**, 104504 (2016).
[2]T. Oyake, L. Feng, T. Shiga, M. Isogawa, Y. Nakamura, and J. Shiomi, Phys. Rev. Lett. **120**, 045901 (2018).
[3]M. Ohnishi and J. Shiomi, APL Mater. **7**, 013102 (2019).
[4]B. Qiu, Z. Tian, A. Vallabhaneni, B. Liao, J. M. Mendoza, O. D. Restrepo, X. Ruan, and G. Chen, EPL **109**, 57006 (2015).
[5]A. J. Minnich, M. S. Dresselhaus, Z. F. Ren, and G. Chen, Energy Environ. Sci. **2**, 466 (2009).
[6]C. Shao, Q. Rong, M. Hu, and H. Bao, J. Appl. Phys. **122**, 155104 (2017).
[7]C. Shao, Q. Rong, N. Li, and H. Bao, Phys. Rev. B **98**, 155418 (2018).
[8]J. Maassen and V. Askarpour, APL Mater. **7**, 013203 (2018).
[9]J. Ravichandran, A. K. Yadav, R. Cheaito, P. B. Rossen, A. Soukiassian, S. J. Suresha, J. C. Duda, B. M. Foley, C.-H. Lee, Y. Zhu, A. W. Lichtenberger, J. E. Moore, D. A. Muller, D. G. Schlom, P. E. Hopkins, A. Majumdar, R. Ramesh, and M. A. Zurbuchen, Nat. Mater. **13**, 168 (2014).
[10]R. Hu, S. Iwamoto, L. Feng, S. Ju, S. Hu, M. Ohnishi, N. Nagai, K. Hirakawa, and J. Shiomi, Phys. Rev. X **10**, 021050 (2020).
[11]M. S. Dresselhaus, G. Chen, M. Y. Tang, R. G. Yang, H. Lee, D. Z. Wang, Z. F. Ren, J.-P. Fleurial, and P. Gogna, Adv. Mater. **19**, 1043 (2007).
[12]S. Alaie, D. F. Goettler, M. Su, Z. C. Leseman, C. M. Reinke, and I. El-Kady, Nat. Commun. **6**, 7228 (2015).
[13]L.-D. Zhao, S.-H. Lo, Y. Zhang, H. Sun, G. Tan, C. Uher, C. Wolverton, V. P. Dravid, and M. G. Kanatzidis, Nature **508**, 373 (2014).
[14]C. Shao and H. Bao, Sci. Rep. **6**, 27492 (2016).
[15]Q.-Y. Fan, R.-L. Yang, W. Zhang, and S.-N. Yun, Results Phys. **15**, 102580 (2019).
[16]A. J. Bullen, K. E. O'Hara, D. G. Cahill, O. Monteiro, and A. von Keudell, J. Appl. Phys. **88**, 6317 (2000).
[17]S. Ganguly, N. Kazem, D. Carter, and S. M. Kauzlarich, J. Am. Chem. Soc. **136**, 1296 (2014).
[18]H. Zhang, H. Liu, K. Wei, O. O. Kurakevych, Y. Le Godec, Z. Liu, J. Martin, M. Guerrette, G. S. Nolas, and T. A. Strobel, Phys. Rev. Lett. **118**, 146601 (2017).
[19]Y. Ikoma, Mater. Trans. **60**, 1168 (2019).
[20]R. Z. Valiev, Y. Estrin, Z. Horita, T. G. Langdon, M. J. Zehetbauer, and Y. T. Zhu, JOM **58**, 33 (2006).
[21]Y. Ikoma, K. Hayano, K. Edalati, K. Saito, Q. Guo, and Z. Horita, Appl. Phys. Lett. **101**, 121908 (2012).
[22]Y. Fukushima, Y. Ikoma, K. Edalati, B. Chon, D. J. Smith, and Z. Horita, Mater. Charact. **129**, 163 (2017).
[23]B. Chon, Y. Ikoma, M. Kohno, J. Shiomi, M. R. McCartney, D. J. Smith, and Z. Horita, Scr. Mater. **157**, 120 (2018).
[24]H. R. Jafarian and M. F. Tarazkouhi, Mater. Sci. Eng. A **686**, 113 (2017).
[25]S. Harish, M. Tabara, Y. Ikoma, Z. Horita, Y. Takata, D. G. Cahill, and M. Kohno, Nanoscale Res. Lett. **9**, 326 (2014).
[26]Y. Ikoma, B. Chon, T. Yamasaki, K. Takahashi, K. Saito, Q. Guo, and Z. Horita, Appl. Phys. Lett. **113**, 101904 (2018).
[27]H. Abe, Teion Kogaku **50**, 314 (2015).
[28]P. Giannozzi, S. Baroni, N. Bonini, M. Calandra, R. Car, C. Cavazzoni, D. Ceresoli, G. L. Chiarotti, M. Cococcioni, I. Dabo, A. D. Corso, S. de Gironcoli, S. Fabris, G. Fratesi, R. Gebauer, U. Gerstmann, C. Gougoussis, A. Kokalj, M. Lazzeri, L. Martin-Samos, N. Marzari, F. Mauri, R. Mazzarello, S. Paolini, A. Pasquarello, L. Paulatto, C. Sbraccia, S. Scandolo, G. Sclauzero, A. P. Seitsonen, A. Smogunov, P. Umari, and R. M. Wentzcovitch, J. Phys. Condens. Matter. **21**, 395502 (2009).
[29]T. Tadano, Y. Gohda, and S. Tsuneyuki, J. Phys. Condens. Matter. **26**, 225402 (2014).
[30]J. M. Ziman, *Electrons and Phonons: The Theory of Transport Phenomena in Solids* (Oxford University Press, Clarendon, Oxford, 1960).
[31]T. Hori, J. Shiomi, and C. Dames, Appl. Phys. Lett. **106**, 171901 (2015).
[32]E. T. Swartz and R. O. Pohl, Rev. Mod. Phys. **61**, 605 (1989).
[33]T. C. Choy, *Effective Medium Theory: Principles and Applications* (Oxford University Press, 2015).
[34]K. Pietrak and T. S. Wiśniewski, J. Power Technol. **95**, 14 (2014), available at http://papers.itc.pw.edu.pl/index.php/JPT/article/view/463.

[35]Y. Ikoma, K. Hayano, K. Edalati, K. Saito, Q. Guo, Z. Horita, T. Aoki, and D. J. Smith, J. Mater. Sci. **49**, 6565 (2014).

[36]C.-W. Nan, R. Birringer, D. R. Clarke, and H. Gleiter, J. Appl. Phys. **81**, 6692 (1997).

[37]J. Ordóñez-Miranda, J. J. Alvarado-Gil, and R. Medina-Ezquivel, Int. J. Thermophys. **31**, 975 (2010).

[38]B. Jugdersuren, B. T. Kearney, D. R. Queen, T. H. Metcalf, J. C. Culbertson, C. N. Chervin, R. M. Stroud, W. Nemeth, Q. Wang, and X. Liu, Phys. Rev. B **96**, 014206 (2017).

[39]G. H. Zhu, H. Lee, Y. C. Lan, X. W. Wang, G. Joshi, D. Z. Wang, J. Yang, D. Vashaee, H. Guilbert, A. Pillitteri, M. S. Dresselhaus, G. Chen, and Z. F. Ren, Phys. Rev. Lett. **102**, 196803 (2009).

[40]D. A. Broido, M. Malorny, G. Birner, N. Mingo, and D. A. Stewart, Appl. Phys. Lett. **91**, 231922 (2007).

[41]C. Hua and A. J. Minnich, Semicond. Sci. Technol. **29**, 124004 (2014).

[42]M.-S. Jeng, R. Yang, D. Song, and G. Chen, J. Heat Transfer **130**, 042410 (2008).

[43]L. Yang and A. J. Minnich, Sci. Rep. **7**, 44254 (2017).

[44]Q. Hao, J. Appl. Phys. **111**, 014307 (2012).

[45]T. Shiga and J. Shiomi, Jpn. J. Appl. Phys. **57**, 120312 (2018).

[46]J. Čížek, M. Janeček, T. Vlasák, B. Smola, O. Melikhova, R. K. Islamgaliev, and S. V. Dobatkin, Mater. Trans. **60**, 1533 (2019).

[47]M. Kashiwagi, Y. Sudo, T. Shiga, and J. Shiomi, Phys. Rev. Appl. **10**, 044018 (2018).